Journal of Engineering Mathematics **50:** 223–240, 2004.

Generation of interfacial instabilities in charged electrified viscous liquid films

D.T. PAPAGEORGIOU and P.G. PETROPOULOS
Department of Mathematical Sciences and Center for Applied Mathematics and Statistics, New Jersey Institute of Technology, University Heights, Newark, NJ 07102, USA (depapa@m.njit.edu)

Received 12 March 2004; accepted in revised form 11 August 2004

Abstract. This study is concerned with the stability of a two-dimensional incompressible conducting liquid film surrounded by a passive conducting medium, when an electric field is applied in a direction parallel to the initially flat bounding fluid interfaces. Currents generate charges at the bounding interfaces which in turn affect the stress balances there. In the absence of an electric field, the viscous liquid film is stable (instability can be induced by the inclusion of van der Waals forces for ultra thin films). A complete model is presented, at arbitrary Reynolds number, which accounts for conductivity and permittivity contrasts between the fluid and surrounding medium, as well as surface tension. The linear stability of the system is considered for arbitrary Reynolds numbers and it is shown that the stable film can become unstable if, (i) $\sigma_R \varepsilon_p > 1$, or (ii) $\sigma_R \varepsilon_p < 1$ and $(\sigma_R - 1)(1 - \varepsilon_p) < 0$, where σ_R is the ratio of outer to inner conductivity and ϵ_p is the ratio of inner to outer permittivity. Instability is possible only if the electric field is non-zero and the scalings near bifurcation points that can be used to construct nonlinear theories are calculated. Several asymptotic limits are also considered including zero Reynolds numbers and short or long waves. The instability criteria given above are constructed explicitly in the case of Stokes flow.

Key words: conducting liquid film, electrohydrodynamic instability, leaky dielectric model, linear stability

1. Introduction

Thin liquid films are important in a variety of applications from biophysics and engineering. Instability and rupture of such films and the control of such events is of theoretical and technological interest. Instability and rupture of liquid films can be found in colloid and bicolloid systems and particular applications involve the rupture of soap films, coalescence of emulsions, fusion of lipid bilayers or biological membranes, to mention a few (see for example [1,2] and references therein). Liquid-film flows can also be found in heat and mass transfer processes in different engineering applications.

The stability of liquid films in the absence of electric fields has been studied by many authors, both theoretically using linear theories [3–6], and experimentally (for example [6]). In the absence of viscosity and gravity, exact capillary traveling waves have been found by Kinnersley [7] and additional ones by Crowdy [8]. The Kinnersley solutions were extended by Papageorgiou and Vanden-Broeck [9,10] who included a parallel electric field in the system and a dielectric fluid, and constructed, numerically, symmetric and antisymmetric traveling waves of arbitrary amplitude and wavelength. The study in [9] also derives nonlinear long-wave equations using a method different to, but with the same results, as Tilley *et al.* [11]. The latter study also considers the dynamics and rupture (including finite-time singularity and self-similar structures) of the electrified film and concludes that the electric delays the rupture time.

When viscosity is present, thin liquid films are linearly stable and can evolve nonlinearly to rupture if van der Waals attractive forces are included in the model, for example, as in

[1,2,12,13]. The evolution equations derived in [12] and related problems are considered in [14–17], who study in particular the types of singularities formed near rupture. In the presence of electric fields, we have additional physical effects such as body forces due to currents in conducting fluids, and Maxwell stresses at free interfaces. The inclusion of a parallel electric field on a dielectric fluid has a stabilizing effect; this is shown in [18] who derive nonlinear evolution equations that generalize those of [12]. It is also established that the instability introduced by van der Waals forces can be completely suppressed by a strong enough electric field. Numerical calculations based on the model equations show that the electric field can be used to delay the rupture time or even completely stabilize the flow.

Melcher [19, Chapters 1–2] examined the effect of an electric field on the linear stability of a sharp interface separating two non-conducting dielectric fluids of infinite extent, and finds that the electric field is stabilizing and increases the speed of propagation of surface waves. This behavior continues into the fully nonlinear regime as discovered by the computations of [9,10]. The linear stability of the interface separating two viscous conducting fluids of infinite extent in the presence of an electric field applied parallel to the interface, has been considered in [20]. Various limits are studied and it is established that charge relaxation can induce an instability. Relevant reviews can be found in [21,22]. Also of relevance are the studies of Mestel [23,24] who considers the stability of charged cylindrical jets – in the cylindrical geometry surface tension destabilizes short waves and so plays a different role than it does here. In a more recent experimental and theoretical study, Burcham and Saville [25,26] consider the stability of liquid bridges of a conducting liquid surrounded by a second conducting medium. They show how an electric field can be used to alter the capillary instability of liquid bridges, and make comparisons between theory and experiment. In particular, they indicate how longer stable bridges can be formed in the presence of electric fields. Our study is concerned with the two-dimensional problem where capillary instability is absent and in fact surface tension has a regularizing effect. Thus, we wish to isolate possible interfacial charge related instabilities from the problem and at the same time retain a jet geometry with interfaces bounding a fluid region.

The present study considers the stability of an electrified viscous film under general conditions. The film liquid and surrounding medium are conducting and charges are supported on the interface. The surrounding region is taken to be hydrodynamically passive. Using linear theory, we derive instability criteria when charges are present for arbitrary Reynolds numbers and instability wavelengths. This study forms the basis of a nonlinear theory as in [18], for example, as well as full computations of symmetric and antisymmetric solutions. The paper is organized as follows: Section 2 contains the model and boundary conditions in the most general case. Section 3 formulates the linear stability problem and derives the general dispersion relation which is solved numerically to determine the stability. Several asymptotic limits are also considered and compared with the calculations. The case of zero Reynolds numbers is considered in Section 4 and Section 5 contains our conclusions.

2. Governing equations

Consider a layer of viscous conducting fluid of undisturbed thickness $2d$. The fluid viscosity is μ, its density ρ, its electrical conductivity σ_0 and its permittivity $\varepsilon_0\varepsilon_p$, where ε_0 is the permittivity of the surrounding medium. The surrounding region outside the fluid layer is hydrodynamically passive and has conductivity $\sigma_0\sigma_R$. The undisturbed layer is symmetric about $y=0$ and an electric field acts in the x direction, where a Cartesian coordinate system is adopted and the flow is assumed to be two-dimensional. The bounding interfaces are free to move

and surface tension acts with coefficient γ. The effect of gravity is neglected throughout – we assume that the thickness of the film is sufficiently small so that surface-tension forces dominate.

We begin by stating the mathematical model. We use the so-called leaky dielectric model (see for example [22]) which allows for charge distribution on interfaces due to current fluxes from the bulk. The hydrodynamics are governed by the Navier–Stokes equations and the electric field in regions 1 and 2 is determined by solving Laplace equations for the corresponding voltage potentials (this is valid since we do not have sources of charge in the bulk – any charge which is present will move to the interface in a time-scale which is fast compared to the hydrodynamics). In addition to these field equations, we have a set of nonlinear boundary conditions at the moving interfaces as documented below.

Denoting the velocity field and pressure in region 1 by $\mathbf{u}$ and p (without loss of generality we take the constant pressure in the surrounding medium to be zero), and the voltage potentials by $V^{(i)}$, $i=1,2$, the field equations in dimensional form are:
Fluid dynamics

$$\rho\,(\mathbf{u}_t+\mathbf{u}\cdot\nabla\mathbf{u})=-\nabla p+\mu\nabla^2\mathbf{u}, \tag{1}$$

$$\nabla\cdot\mathbf{u}=0. \tag{2}$$

Voltage potentials

$$\nabla^2 V^{(i)}=0. \tag{3}$$

The boundary conditions at the interface $y=H(x,t)$ are a kinematic condition, continuity of normal and tangential stresses there, continuity of the tangential component of the electric field and either continuity of the current flux, if the fluids are conducting (equivalently conservation of surface charge), or continuity of the normal component of the displacement field ($\varepsilon\mathbf{E}$) for non-conducting fluids. The electric-field conditions are modified further if one of the fluids is conducting and the other is a dielectric (*i.e.,* an insulator), because charge now builds up at the interface and must be tracked as part of the solution.

To discuss the boundary conditions at the interface we use the stress tensor $\mathbf{T}=\mathbf{T}^{\mathrm{f}}+\mathbf{T}^{\mathrm{e}}$ composed of a fluid part $\mathbf{T}^{\mathrm{f}}$ and an electrical part $\mathbf{T}^{\mathrm{e}}$. In tensor notation the stresses are given by,

$$T^{\mathrm{f}}_{ij}=-p\delta_{ij}+\mu\left(\frac{\partial u_i}{\partial x_j}+\frac{\partial u_j}{\partial x_i}\right)\qquad T^{\mathrm{e}}_{ij}=\varepsilon\left(E_iE_j-\frac{1}{2}|\mathbf{E}|^2\delta_{ij}\right), \tag{4}$$

where it is understood that subscripts 1 and 2 are to be used for all variables in (4) as appropriate. We give the general boundary conditions at the interface $\mathbf{X}=x\mathbf{e}_x+H(x,t)\mathbf{e}_y$, where we assume that there exists a surface charge density $q(x,t)$. Different physical limits are discussed later. The following formulation is similar to that in the reviews [21,22,27] (see also [28, Chapters 1–3] for a general discussion of electrostatics):

$$\mathbf{n}\cdot\mathbf{X}_t=\mathbf{n}\cdot\mathbf{u};\quad[\mathbf{n}\cdot(\mathbf{T}^{\mathrm{f}}+\mathbf{T}^{\mathrm{e}})\cdot\mathbf{n}]_2^1=\gamma\nabla\cdot\mathbf{n}; \tag{5,6}$$

$$[\mathbf{t}\cdot\mathbf{T}^{\mathrm{f}}\cdot\mathbf{n}]_2^1=q\mathbf{E}\cdot\mathbf{t};\quad[\mathbf{n}\times\mathbf{E}]_2^1=0;\quad[\mathbf{n}\cdot(\varepsilon\mathbf{E})]_2^1=-q; \tag{7,8,9}$$

$$q_t-\mathbf{X}_t\cdot\nabla_s q+\nabla_s\cdot(q\mathbf{u}_s)+q\kappa\mathbf{u}\cdot\mathbf{n}=\mathbf{n}\cdot[\sigma\mathbf{E}]_2^1, \tag{10}$$

where $[\cdot]_2^1$ denotes the jump in the variable as the interface is crossed from region 1 to region 2, subscripts s denote surface quantities and κ is the curvature. The electric field is expressed

by $\mathbf{E}^{(1,2)} = -\nabla V^{(1,2)}$. The vectors $\mathbf{n} = (-H_x, 1)/(1 + H_x^2)^{1/2}$ and $\mathbf{t} = (1, H_x)/(1 + H_x^2)^{1/2}$ are the outward-pointing unit normal and tangent to the interface, respectively. Equations (5–7) are the kinematic condition, and normal and tangential-stress balances, respectively. Boundary condition (8) states that the tangential electric field is continuous, condition (9) is Gauss's law relating the electric field to the charge and condition (10) is a statement of surface-charge conservation balancing convection and redistribution of charge due to interface stretching (the terms on the left) with the flux onto the interface due to current contributions from the bulk (usually, currents in the bulk are given by $\mathbf{J} = \sigma\mathbf{E} + q\mathbf{u}$ – the latter contribution is a second-order effect, however, and can be dropped consistently; this term is also absent if the charge relaxation time is much smaller than the fluid dynamical time-scale, since all charges reside on the interface, then – see later). Equation (10) is written out in full component form below (see Equation (23)) following the derivation of a related surfactant equation by Papageorgiou [29, pp. 41–88]. Note also that the tangential stress balance contains contributions from the electric field and the viscous stresses are needed to balance these. In the case of perfect conductors or perfect dielectrics, the electrical contributions to (7) vanish because $\mathbf{E}\cdot\mathbf{t}$ is zero for perfect conductors, and $q = 0$ for perfect dielectrics. Finally, we note an equivalent form of the tangential stress balance equation that clarifies the emergence of (7) and is more appropriate in some limiting forms considered below. The tangential stress balance is $[\mathbf{t}\cdot(\mathbf{T}^{\mathrm{f}} + \mathbf{T}^{\mathrm{e}})\cdot\mathbf{n}]_2^1 = 0$, and the electric part can be manipulated to yield

$$[\mathbf{t}\cdot\mathbf{T}^{\mathrm{f}}\cdot\mathbf{n} + (\varepsilon\mathbf{E}\cdot\mathbf{n})(\mathbf{E}\cdot\mathbf{t})]_2^1 = 0, \tag{11}$$

which on use of the continuity of the tangential component of the electric field (8) and Gauss's law (9), immediately yields (7). The form (11) is useful in analyzing situations where the charge relaxation time is asymptotically small, as we describe later.

The non-dimensionalize variables are as follows (dimensionless quantities are primed but the primes are dropped from the final equations):

$$\begin{aligned} &(x, y) = (\mathrm{d}x', \mathrm{d}y'), \qquad H(x,t) = \mathrm{d}H'(x', y'), \qquad t = \frac{\mathrm{d}\mu}{\gamma}t', \\ &V^{(1,2)} = V_0 V^{(1,2)\prime}, \qquad \mathbf{u} = \frac{\gamma}{\mu}\mathbf{u}', \qquad p = \frac{\gamma}{d}p', \quad q = \frac{\varepsilon_0 V_0}{d}q' \end{aligned} \tag{12}$$

where V_0 is a typical voltage drop driving the base electric field.

Using the relationship $\mathbf{E}^{(\mathbf{1,2})} = -\nabla V^{(1,2)}$ and the scales above, leads to the following dimensionless problem (written in full component form) and boundary conditions:
Field equations

$$R_e\left[u_t + uu_x + vu_y\right] = -p_x + u_{xx} + u_{yy}, \tag{13}$$

$$R_e\left[v_t + uv_x + vv_y\right] = -p_y + v_{xx} + v_{yy}, \tag{14}$$

$$u_x + v_y = 0, \tag{15}$$

$$\nabla^2 V^{(j)} = 0, \quad j = 1, 2. \tag{16}$$

As noted earlier we seek solutions which are symmetric about $y = 0$ and this implies

$$u_y(x, 0, t) = v(x, 0, t) = V_y^{(1)}(x, 0, t) = 0. \tag{17}$$

The boundary conditions at the free interface $y = H(x, t)$ are:
Kinematic

$$v = H_t + uH_x. \tag{18}$$

Tangential stress balance

$$2H_x(v_y-u_x)+\left(1-H_x^2\right)(u_y+v_x)=-E_bq\left(V_x^{(1)}+H_xV_y^{(1)}\right). \tag{19}$$

Normal stress balance

$$-p+\frac{2}{\left(1+H_x^2\right)}\left[u_x\left(H_x^2-1\right)-H_x(u_y+v_x)\right]$$
$$+\frac{E_b}{(1+H_x^2)}\left[\left(1-H_x^2\right)\left[\frac{\varepsilon}{2\varepsilon_0}\left(V_y^2-V_x^2\right)\right]_2^1-2H_x\left[\frac{\varepsilon}{\varepsilon_0}V_xV_y\right]_2^1\right]=\frac{H_{xx}}{\left(1+H_x^2\right)^{3/2}}, \tag{20}$$

where it is understood that quantities in square brackets are evaluated with the variables corresponding to the appropriate region.

Continuity of tangential electric field

$$H_xV_y^{(1)}+V_x^{(1)}=H_xV_y^{(2)}+V_x^{(2)}; \tag{21}$$

Gauss's law

$$\varepsilon_p\left(H_xV_x^{(1)}-V_y^{(1)}\right)-\left(H_xV_x^{(2)}-V_y^{(2)}\right)=-q\sqrt{1+H_x^2}; \tag{22}$$

Conservation of interfacial charge

$$q_t-\frac{H_tH_x}{\left(1+H_x^2\right)}q_x+\frac{1}{\sqrt{1+H_x^2}}\left(\frac{(u+vH_x)q}{\sqrt{1+H_x^2}}\right)_x+\frac{q(v-uH_x)H_{xx}}{\left(1+H_x^2\right)^2}$$
$$=-\frac{T}{\left(1+H_x^2\right)^{1/2}}\left[V_y^{(1)}-H_xV_x^{(1)}-\sigma_R\left(V_y^{(2)}-H_xV_x^{(2)}\right)\right]. \tag{23}$$

The dimensionless parameters that appear in the model are a Reynolds number R_e (proportional to the Ohnesorge number), an electric Weber number E_b measuring the ratio of electric to capillary pressures, the ratio of fluid to electric time-scales T and σ_R, ε_p introduced earlier. These are given by

$$R_e=\frac{\rho\gamma d}{\mu^2},\qquad E_b=\frac{\varepsilon_0V_0^2}{\gamma d},\quad T=\frac{\tau^F}{\tau^E}=\frac{(\mu d/\gamma)}{(\varepsilon_0/\sigma_0)},\quad \sigma_R=\frac{\sigma_{\text{out}}}{\sigma_{\text{in}}},\quad \varepsilon_p=\frac{\varepsilon_{\text{in}}}{\varepsilon_{\text{out}}}. \tag{24}$$

We note that this choice of scales is the same as that used by Burcham and Saville [26]. It is also useful to consider typical sizes of the dimensionless parameters found in available experiments. In the microgravity liquid bridge experiments of Burcham and Saville [25], physical properties of different fluids used are given in their Table 1. By analogy, if we consider a liquid-film of thickess 5 mm, then that data can be used to estimate typical values of the Reynolds number R_e; for example, silicone oil 12 M at 25 °C has $R_e\approx 0{\cdot}01$ while silicone oil 1 M has $R_e\approx 0{\cdot}1$. Higher values can be achieved for different fluids but in all cases R_e is small or order one (the linear theory of [26] is carried out at zero R_e). For completeness, however, we consider the stability problem at arbitrary values of R_e as large as 500. Of interest also are the values of the ratio of time-scales T, defined above. For the experiments just mentioned, the values of T are approximately 10 and 24 respectively, justifying the assumption of fast charge relaxation times adopted later – see also Burcham and Saville [25,26].

Specification of initial and boundary conditions provides a nonlinear moving-boundary problem which must, in general, be addressed numerically. As far as we know this nonlinear

problem has not been studied and we proceed with a linear stability analysis in order to identify the types of instabilities that are possible as well as to obtain information regarding the well-posedness of the system. We note that in general $R_e = O(1)$ in which case the underlying numerical problem cannot be addressed using boundary-integral methods which have been successful for moving-interface problems (see Pozrikidis [30]). The Stokes-flow limit is a special case and follows readily from our non-dimensionalization by considering asymptotically $R_e \to 0$ in Equations (13–14).

2.1. Fast charge relaxation times

Typically the parameter T which measures the ratio of fluid to charge relaxation time-scales, is large and we consider the limiting form of the equations for $T \gg 1$. Similar assumptions are made in the studies of Burcham and Saville [26] and Pelekasis *et al.* [31]. It can be seen from (23) that for large T we obtain

$$[\sigma \mathbf{E} \cdot \mathbf{n}]_2^1 = 0, \tag{25}$$

which physically implies that the current normal to the interface is continuous. In addition, the charge q on the interface can be determined from the identity (9) once the problem has been solved. The appropriate tangential stress condition is now (11) which is given in its full form below:

$$2H_x(v_y - u_x) + \left(1 - H_x^2\right)(u_y + v_x) = E_b\left(V_x^{(1)} + H_x V_y^{(1)}\right)\left[\varepsilon_p\left(H_x V_x^{(1)} - V_y^{(1)}\right) - \left(H_x V_x^{(2)} - V_y^{(2)}\right)\right]. \tag{26}$$

The large T limit consists of the field equations (13–16) and the boundary conditions (17–18), (20) and (25–26). Note that the charge at the interface can be determined afterwards from (22).

In the remainder of the article we consider the stability characteristics of the problem in the limit of small charge relaxation times. As noted earlier, the $q\mathbf{u}$ contribution in the expression for the current in the bulk, is negligible in this limit since charges move onto the interface with a very fast time-scale leaving zero charge behind, to leading order.

3. Linear stability

The flat film is an equilibrium state of the equations and boundary conditions. More specifically, this base state is (we use bars to denote it)

$$\bar{H} = 1, \qquad \bar{\mathbf{u}} = 0, \qquad \nabla \bar{V}^{(1)} = \nabla \bar{V}^{(2)} = -\mathbf{e}_x, \qquad \bar{p} = \frac{1}{2} E_b (1 - \varepsilon_p), \qquad \bar{q} = 0. \tag{27}$$

We add perturbations, decorated with a tilde, and linearize the field equations and boundary conditions to obtain the following problem:

$$R_e \tilde{u}_t = -\tilde{p}_x + \nabla^2 \tilde{u}, \quad R_e \tilde{v}_t = -\tilde{p}_y + \nabla^2 \tilde{v}, \tag{28, 29}$$

$$\tilde{u}_x + \tilde{v}_y = 0, \quad \nabla^2 \tilde{V}^{(1)} = \nabla^2 \tilde{V}^{(2)} = 0. \tag{30, 31}$$

The symmetry boundary conditions at $y = 0$ are identical to (17) but for tilde variables, and the boundary conditions at $y = 1$ become:

$$\tilde{v} = \tilde{H}_t, \qquad \tilde{u}_y + \tilde{v}_x = E_b\left[(\varepsilon_p - 1)\tilde{H}_x + \varepsilon_p \tilde{V}_y^{(1)} - V_y^{(2)}\right], \tag{32, 33}$$

$$-\tilde{p} - 2\tilde{u}_x - E_b\left(\tilde{V}_x^{(2)} - \varepsilon_p \tilde{V}_x^{(1)}\right) = \tilde{H}_{xx}; \tag{34}$$

$$\tilde{V}_x^{(1)} = \tilde{V}_x^{(2)}, \qquad \tilde{H}_x + \tilde{V}_y^{(1)} - \sigma_R\left(\tilde{H}_x + \tilde{V}_y^{(2)}\right) = 0. \tag{35, 36}$$

The distrurbance charge follows from the linearized version of Gauss's law (22),

$$\tilde{q} = (\varepsilon_p - 1)\tilde{H}_x - \tilde{V}_y^{(2)} + \varepsilon_p \tilde{V}_y^{(1)}. \tag{37}$$

Normal mode solutions are sought in the form

$$\tilde{f}(x, y, t) = \hat{f}(y)\exp(\mathrm{i}kx + \omega t) + c.c., \tag{38}$$

where $c.c.$ denotes complex conjugate, $\tilde{f}$ denotes any of the dependent variables, the wavenumber k is real and stability or instability is determined by the sign of the real part of the eigenvalue ω. The solutions to Equations (28–30) are obtained by elimination of $\hat{p}$ and $\hat{u}$ in favor of $\hat{v}$ to give

$$\hat{v}(y) = \alpha_1 \sinh(ky) + \alpha_2 \sinh(\beta y), \tag{39}$$

where

$$\beta^2 = k^2 + \omega R_e, \tag{40}$$

and α_i with i an integer will denote constants. The voltage perturbations are

$$\hat{V}^{(1)}(y) = \alpha_3 \cosh(ky), \qquad \hat{V}^{(2)}(y) = \alpha_4 \exp(-|k|y). \tag{41}$$

We note that the symmetry conditions have been used in deriving (39) and (41), and the remaining boundary conditions provide five linear homogeneous equations for the unknowns $\mathbf{x} = (\alpha_1, \alpha_2, \alpha_3, \alpha_4, \hat{H})^t$. It is useful to eliminate α_4 in favor of α_3 using condition (35), and in turn to eliminate α_3 in terms of $\hat{H}$ using the linearized current continuity relation (36). This reduces the problem to three homogeneous equations for the three unknowns $\alpha_1, \alpha_2, \hat{H}$. In matrix form this is

$$A\mathbf{x} = 0, \tag{42}$$

with the matrix A given by

$$A = \begin{pmatrix} \sinh k & \sinh\beta & -\omega \\ 2k^2 \sinh k & (\beta^2 + k^2)\sinh\beta & -\Lambda_1 \\ (\beta^2 + k^2)\cosh k & 2k\beta\cosh\beta & k^3 + \Lambda_2 \end{pmatrix} \tag{43}$$

where Λ_1 and Λ_2 are given by

$$\Lambda_1 = \frac{k^2 e^k E_b(\varepsilon_p \sigma_R - 1)}{\eta}, \qquad \Lambda_2 = \frac{k^2 \cosh(k)}{\eta}(\sigma_R - 1)(1 - \varepsilon_p)E_b. \tag{44}$$

For non-trivial solutions of (42) we have $\det(A) = 0$ leading to the following dispersion relation:

$$\begin{aligned}(2k^2 + \omega R_e)\coth(k)\left[\omega^2 R_e + 2k^2\omega - \Lambda_1\right] \\ +2k\beta\coth\beta\left[\Lambda_1 - 2k^2\omega\right] + \omega R_e\left[k^3 + \Lambda_2\right] = 0.\end{aligned} \tag{45}$$

The quantity η is

$$\eta = \sinh k + \sigma_R \cosh k. \tag{46}$$

The root-finding problem (45) is slightly complicated due to the implicit appearance of ω in the dispersion relation through β. We used Mathematica to calculate branches of the dispersion relation and confirmed that for $E_b = 0$ we reproduce the results in [18]; the flow is stable for all wavenumbers then. Unless otherwise noted, ω remains real (to within machine precision and truncation error) and growth or decay are identified by $\omega > 0$ or $\omega < 0$, respectively.

Before presenting general stability charecteristics, it is useful to consider the asymptotic limits of long and short waves characterized by $k \ll 1$ and $k \gg 1$, respectively. The behavior as $k \to 0$ for fixed R_e, E_b, ε_p and σ_R, follows readily from (45) and is found to have the form $\omega = k\omega_1 + k^2\omega_2 + \cdots$, where

$$\omega_1^2 = \frac{E_b(\varepsilon_p\sigma_R - 1)}{\sigma_R R_e} \Rightarrow \omega = \pm\left[\frac{E_b(\varepsilon_p\sigma_R - 1)}{\sigma_R R_e}\right]^{1/2} k + \cdots, \tag{47}$$

showing that real roots and consequently instability, is possible if

$$\varepsilon_p\sigma_R > 1. \tag{48}$$

It has been found from extensive calculations that the condition (48) is sufficient but not necessary for instability (it is clearly necessary for long wave instability). When $\varepsilon_p\sigma_R < 1$ long waves are neutrally stable and have non-zero frequencies equal to $\sqrt{E_b|\varepsilon_p\sigma_R|/(\sigma_R R_e)}$. It is possible, however, to obtain instability at higher wavenumbers if the parameters satisfy certain constraints. As we show later when we analyze the zero Reynolds number limit in detail, instability at $k = O(1)$ can be found even when (48) is not satisfied as long as the additional condition

$$(\sigma_R - 1)(1 - \epsilon_p) < 0, \tag{49}$$

is simultaneously satisfied. This behavior carries over to non-zero R_e and we illustrate such a case below. The second condition (49) is in agreement with that of Melcher and Schwarz [20], who also point out that its origin is due to the polarization force at the interface due to the difference in permittivities. Note, however, that condition (49) requires pairs of fluids with the property that the fluid of higher conductivity has a lower permittivity or vice versa, which is hard to achieve in practice (see [20]). If (48) is satisfied, a damped root also emanates from the origin and has negative growth rate for all k. If the criterion (48) is not satisfied, then it has been confirmed numerically that there are no growing modes for wide ranges of parameters.

For large k, the roots take the form $\omega = k^2\omega_2 + k\omega_1 + \omega_0 + \cdots$, from which it follows that the leading-order contribution from (45) gives the following polynomial for ω_2:

$$(2 + \omega_2 R_e)^4 = 16(1 + \omega_2 R_e). \tag{50}$$

One root is $\omega_2 = 0$ and using elementary methods it is easy to establish that there exists another real root of (50) in the interval $-1/R_e < \omega_2 < 0$, which provides short wave damping proportional to $-k^2$; the root is approximately given by

$$\omega \approx -\frac{0{\cdot}9126}{R_e}k^2, \quad k \gg 1. \tag{51}$$

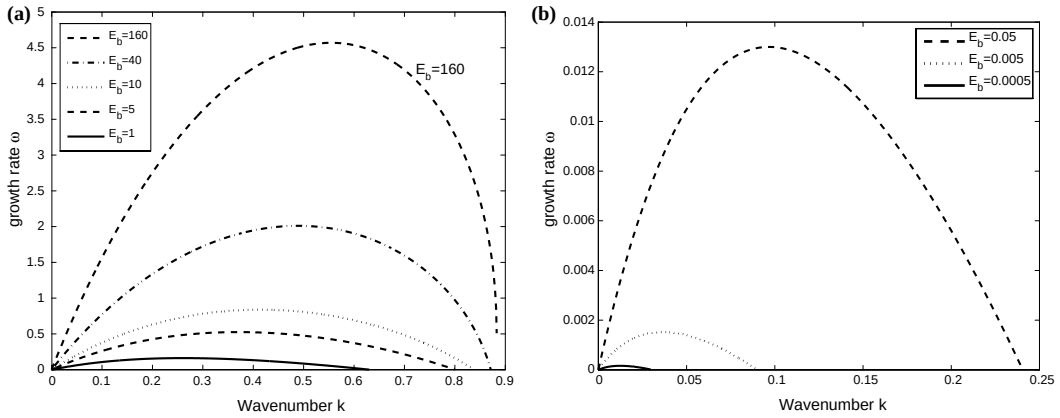

Figure 1. (a) Unstable modes for $R_e = 1$, $\varepsilon_p = 4$, $\sigma_R = 0{\cdot}5$; E_b varies from 160 to 1. (b) Unstable modes for lower $E_b = 0{\cdot}05$, $0{\cdot}005$, $0{\cdot}0005$.

Guided by the calculations presented later, it is relevant to consider the situation $\omega_2 = 0$ and to calculate ω_1 and at the next order ω_0 from the dispersion relation. The result is

$$\omega \approx -\frac{1}{2}k + \left[-\frac{3R_e}{16} - \frac{(\sigma_R - 1)(1-\varepsilon_p)E_b}{2(1+\sigma_R)}\right], \qquad k \gg 1. \tag{52}$$

Short waves are damped, therefore, as would be expected. The quadratic behavior given by (51) is associated with the short wave limit of the damped root emanating from the origin, while the linear behavior (52) corresponds to the short wave limit of the growing root – see below.

Representative numerical results when (48) is satisfied, are presented in Figures 1–6. There are four dimensionless parameters in the problem, the Reynolds number R_e, the permittivity and conductivity ratios ε_p and σ_R, and the electric field parameter (electric Weber number), E_b. Figure 1 fixes the values $R_e = 1$, $\varepsilon_p = 4$ and $\sigma_R = 0{\cdot}5$ and presents the stability characteristics as E_b varies. It can be seen that for the given choice of parameters the instability decreases with decreasing E_b and in fact disappears completely in the absence of an electric field since viscous damping is the only effect then. Another notable feature of Figure 1 is that both the maximum growth rate and the size of the band of unstable waves decrease to zero in the limit $E_b \to 0$. The precise rate at which this happens is critical in constructing a weakly nonlinear theory for small E_b and our results can be used to identify these scalings. Considering the results in Figure 1, the maximum growth rates when $E_b = 0{\cdot}05$, $0{\cdot}005$, $0{\cdot}0005$, are approximately equal to $0{\cdot}013$, $0{\cdot}0015$, $0{\cdot}00016$, while the corresponding critical wavenumbers, k_c say (*i.e.*, the wavenumber above which the flow is stable), are approximately $0{\cdot}24$, $0{\cdot}09$, $0{\cdot}03$, respectively. Noting that E_b is decreased by a factor of 10 in each instance, we obtain evidence of the scalings

$$\omega_{\max} \sim E_b, \quad k_c \sim \sqrt{E_b} \qquad \text{as} \quad E_b \to 0. \tag{53}$$

These have been confirmed asymptotically also starting with (45) and lead to the scalings required to construct a weakly nonlinear theory. We do not pursue the nonlinear analysis here but leave it for future work coupled with strongly nonlinear calculations.

We present next a more detailed picture of the modes for the case $E_b = 1$, the other parameters being those of Figure 1. As indicated by the asymptotic results (47–52), there is one stable and one unstable root in the vicinity of $k = 0$. A comparison between the asymptotic

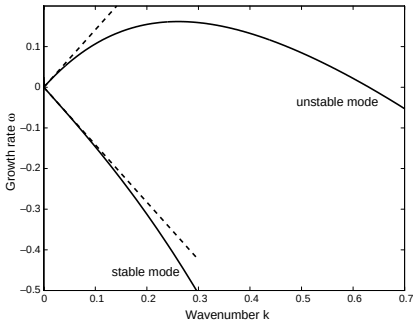

Figure 2. Comparison of calculated modes (solid) and asymptotic results for long waves (dashed) given by (47). Parameter values are: $E_b = 1$, $R_e = 1$, $\varepsilon_p = 4$ and $\sigma_R = 0{\cdot}5$.

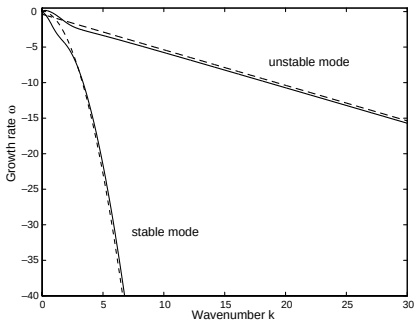

Figure 3. Comparison of calculated modes (solid) and asymptotic results for short waves (dashed) given by (51) (stable mode), and (52) (unstable mode). Parameter values are: $E_b = 1$, $R_e = 1$, $\varepsilon_p = 4$ and $\sigma_R = 0{\cdot}5$.

results (47) and the calculated growth rates are given in Figure 2. The linear behavior predicted by the asymptotic formulas (dashed lines) are in excellent agreement with the calculated modes (solid curves). The unstable mode becomes stable at large enough wavenumbers and we consider the large k asymptotic behavior of both modes in Figure 3, where again asymptotic predictions are indicated with dashed curves. It is clear from the results that the unstable mode decays linearly with k while the decay of the stable mode has a faster quadratic decay rate with k. The corresponding asymptotic predictions (51) and (52) are superimposed and agreement is again very good. (Note that the excellent agreement for the stable mode was verified for values of k as large as 30, but the results are not depicted due to the scale of the relatively rapid decay.)

We consider next the effect of the ratio of conductivities on the stability of the layer. The other parameters are fixed at $R_e = 1$, $E_b = 10$ and $\varepsilon_p = 4$, and results are presented in Figure 4 as σ_R, the ratio of the outer to the inner conductivity, is reduced. Figure 4a presents results for $\sigma_R > 1$ and Figure 4b corresponds to $\sigma_R < 1$. In both cases, we observe a reduction of the instability as σ_R decreases, with a decrease in both maximum growth rate ($\omega_{\max}$) and critical wavenumber (k_c) being evident. In fact, the instability disappears completely for

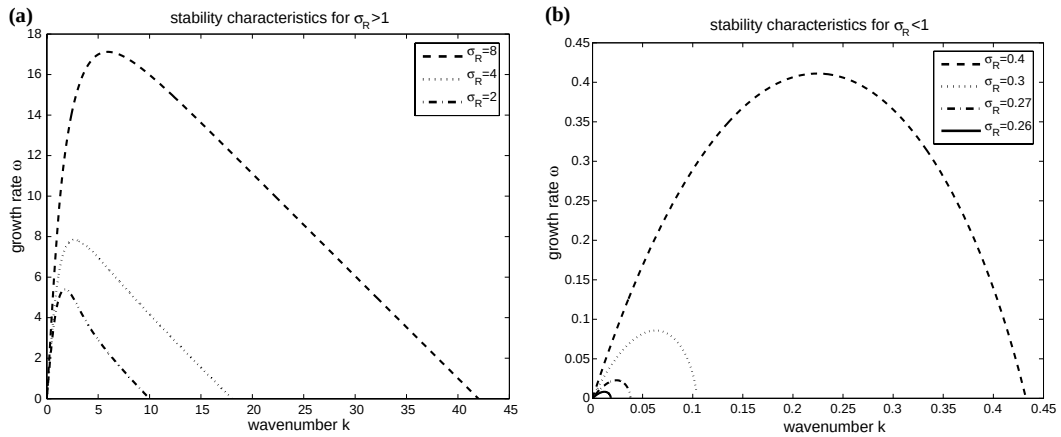

Figure 4. (a) Unstable modes for $\sigma_R > 1$ (values given in the figure); $R_e = 1$, $E_b = 10$, $\varepsilon_p = 4$. (b) Unstable modes for $\sigma_R < 1$ (values given in the figure); same parameters as in (a).

$\sigma_R < \sigma_{Rc} = 1/4$ (this is criterion (48)), with both $\omega_{\max}$ and k_c tending to zero as $\sigma_R \to \sigma_{Rc}+$. The rates at which $\omega_{\max}$ and k_c tend to zero as a function of the small parameter $(\sigma_R - \sigma_{Rc})$ are useful in the construction of the appropriate scalings that lead to a weakly nonlinear theory, in much the same way as was discussed above for the limit $E_b \to 0$. In the table below we present numerical evidence of such scalings from calculations near the stability limit $\sigma_{Rc} = 0{\cdot}25$.

Table 1.

σ_R	$\sigma_R - 0{\cdot}25$	$\omega_{\max}$	k_c	$\omega_{\max}$ ratio	k_c ratio
0·3	0·05	0·086	0·104	–	–
0·255	0·005	0·003	0·009	28·7	11·5
0·2505	0·0005	$9{\cdot}6\times10^{-5}$	9×10^{-4}	31·5	10
0·25005	0·00005	$3{\cdot}05\times10^{-6}$	9×10^{-5}	31·5	10

The table contains values of $\omega_{\max}$ and k_c as the value of $\sigma_R - (1/4)$ is successively decreased by a factor of 10 starting at 0·3 and ending at 0·25005. The last two columns in the table show the corresponding decrease of $\omega_{\max}$ and k_c; noting that $10^{3/2} \approx 31{\cdot}6$, it can be concluded that $\omega_{\max}$ behaves like $(\sigma_R - \sigma_c)^{3/2}$, and k_c decreases by a factor of 10 each time and therefore behaves like $(\sigma_R - \sigma_c)$. Guided by the calculations, this asymptotic result can be established by considering the behavior of (45) in the double limit $\omega \to 0$, $k \to 0$ where a main balance is found with contributions from the first two terms. In conclusion, then, we have the following asymptotic behavior which can be used to construct the nonlinear evolution of the flow in the neighborhood of the bifurcation point σ_{Rc} (the fact that $\sigma_{Rc} = 1/4$ in this numerical example is irrelevant; the behavior is generic) by introducing long spatial and time-scales X and τ, say, according to:

$$X = (\sigma_R - \sigma_{Rc})x, \qquad \tau = (\sigma_R - \sigma_{Rc})^{3/2}t. \tag{54}$$

We do not pursue the nonlinear analysis here but note that it is interesting to compare the weakly nonlinear behavior near the distinct bifurcation points $E_b = 0$ and $\sigma_R = \sigma_{Rc}$, as well as the case when they occur simultaneously.

The effect of variations in the permittivity ratio ε_p is summarized in Figure 5, the other parameters fixed at $R_e = 1$, $E_b = 10$, $\sigma_R = 0{\cdot}5$. As shown asymptotically earlier, a necessary condition for long-wave instability is $\varepsilon_p \sigma_R > 1$; this suggests that for the parameters of Figure 5, we obtain stability (and in fact to all wavenumbers) for $\varepsilon_p < 2$. These observations are in complete agreement with the modes shown in the figure, and again there is a shrinking of the unstable branch as the critical value of ε_p is approached from above. One can again pursue a weakly nonlinear analysis in the neighborhood of the bifurcation point but this is similar to that outlined above pertaining to variations in conductivity and is omitted.

The effect of Reynolds number is considered next. Figure 6 shows stability results as the Reynolds number increases from 10 to 500. The maximum growth rate decreases with R_e and it has been established that the behavior scales with $R_e^{-1/2}$ for large R_e. At the same time, the band of unstable waves is retained and does not shift to asymptotically long waves. Physically we do not expect such large Reynolds numbers for this class of problems (see [25,26]) and Figure 6 is included for completeness. Of more relevance, however, is the zero R_e limit and this is taken up next.

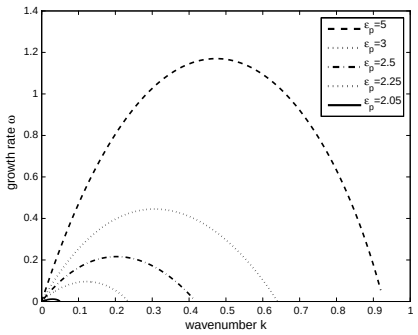

Figure 5. Stability characteristics for different values of the permittivity ratio ε_p. Other parameters are fixed at $R_e = 1$, $E_b = 10$ and $\sigma_R = 0{\cdot}5$.

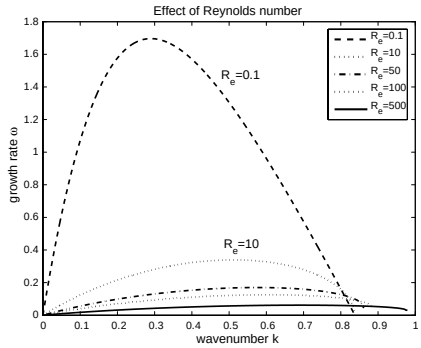

Figure 6. Stability characteristics for different Reynolds numbers. Other parameters are fixed at $E_b = 10$, $\varepsilon_p = 4$ and $\sigma_R = 0{\cdot}5$.

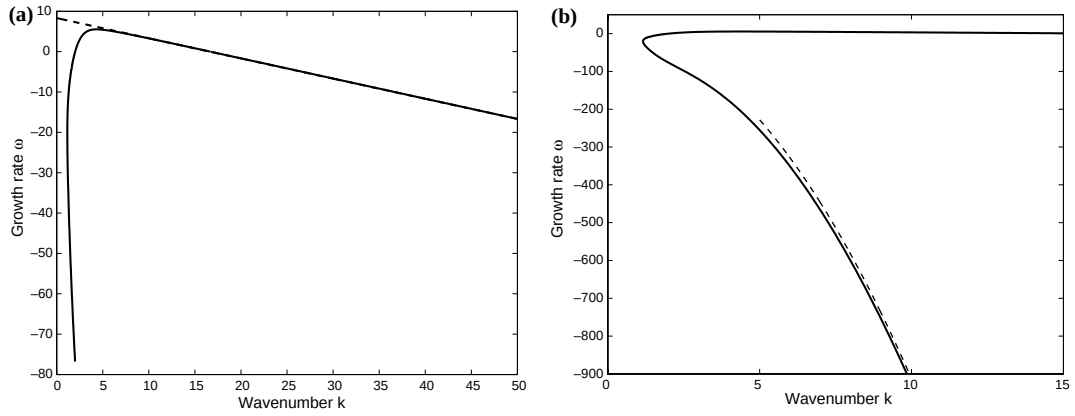

Figure 7. (a) Modes for $Re = 0{\cdot}1$, $\varepsilon_p = 0{\cdot}5$, $\sigma_R = 0{\cdot}5$, $E_b = 100$. Instability is seen over a finite band of wavenumbers and long waves are neutrally stable. The dashed line is the asymptotic result (52). (b) Details of the stable mode structure. The left branch decays fast and the dashed line represents the asymptotic result (51). Same parameters as in (a).

Finally, we consider situations that are characterized by $\varepsilon_p \sigma_R < 1$. It has already been shown that the flow is stable for long waves with the leading-order behavior being a traveling wave with speed that increases as the electric Weber number E_b increases (see (47)). In our numerical search for growing modes we could not obtain instability unless the additional condition (49) is satisfiled (we show this analytically for the Stokes-flow problem). In order to complete the picture of the different modes, we present results for $\varepsilon_p = \sigma_R = 0{\cdot}5$ so that $\varepsilon_p \sigma_R < 1$ but $(\sigma_R - 1)(1 - \varepsilon_p) < 0$, and a non-zero Reynolds number $R_e = 0{\cdot}1$ (other values give qualitatively similar results). The results are shown in Figure 7. Figure 7a details the unstable part of the mode and it is seen that instability is possible for a band of wavenumbers away from $k = 0$. Figure 7b shows the behavior as we move into the lower half plane. All values of ω presented in the figure are real and in the gap to the left of the mode ω is purely imaginary – no roots with a non-zero real part were found there. The figures contain the large k asymptotic results also, and agreement is seen to be very good. The right branch decays according to the linear rate (52) while the left branch has a quadratic decay rate as given by (51). These trends are similar to the decay of the modes for cases having $\varepsilon_p \sigma_R > 1$ – see Figure 3. In fact,

by comparison with Figure 2, we can conclude that when $\varepsilon_p\sigma_R$ decreases below 1 and long waves become neutrally stable, the stable and unstable modes emanating from the origin in Figure 2 merge and move to the right to give the structures shown in Figure 7. It is interesting to note that for a given set of parameters it is possible to have waves which neither grow nor decay but simply translate with a constant speed. For the values of Figure 7, any wave with $k < 1{\cdot}16$, *i.e.*, longer than $2\pi/1{\cdot}16$, is neutrally stable and nonlinear traveling waves may be possible in such regimes.

4. Zero-Reynolds-number limit

It can be seen from the definition of β, Equation (40), that the solutions for the perturbation velocity (39), become linearly dependent if $R_e = 0$; the streamfunction for this two-dimensional Stokes problem satisfies $\nabla^4\psi = 0$ and the symmetry conditions yield the linearly independent solutions $\sinh ky$ and $y\cosh ky$. It is easy to check from (39) that these are the solutions obtained to order R_e as $R_e \to 0$. As expected, therefore, this limit can be applied directly to the dispersion relation (45). Writing $\omega = \omega_0 + R_e\omega_1 + \cdots$, we find that the leading-order term in (45) is $O\left(R_e^0\right)$ and vanishes identically, while at order R_e we obtain the following explicit expression for ω_0:

$$\omega_0 = \frac{E_b(\varepsilon_p\sigma_R - 1)k^3e^k - \eta k^3\sinh^2 k - E_b(\sigma_R - 1)(1-\varepsilon_p)k^2\sinh^2 k\cosh k}{2k^2\eta(\sinh k\cosh k + k)}. \tag{55}$$

It follows directly from (55), that

$$\lim_{k\to 0}\omega_0(k) = \frac{E_b(\varepsilon_p\sigma_R - 1)}{4\sigma_R}, \tag{56}$$

while the short wave limit becomes

$$\omega_0 \sim -\frac{1}{2}k + \ldots, \quad as \;\; k \to \infty, \tag{57}$$

showing that short waves are damped as expected. It is clear from (56) that a necessary condition for long wave instability is $\varepsilon_p\sigma_R > 1$ as was concluded earlier. A comparison between calculated stability characteristics and the asymptotic result (56) is given in Figure 8 for successively decreasing Reynolds numbers. It is seen that agreement is very good and notably the shift of the most unstable wavenumber to zero. We note in passing that a lack of a long wavenumber cut-off is observed in the related problem of capillary instability of a highly viscous liquid jet (see the classical reference [32] and the recent and detailed study of Timmermans and Lister [33]). A long wave cut-off can be obtained in a consistent way starting from the asymptotic scheme introduced above and noting that the result (56) is valid as long as $k^2 \ll R_e$ – this can be seen from the approximation of β for small R_e. In the neighborhood of $k = 0$, then, an inner region must be introduced with $k \sim R_e^{1/2}$ in order to account for the non-uniformity in the expansion. We refer the reader to the analogous liquid thread problem analyzed in detail in [33].

4.1. Neutral stability characteristics

Neutral stability for $R_e = 0$ is achieved by setting $\omega_0 = 0$ in (55). The explicit form of (55) shows that the principle of exchange of stabilities holds in this case, that is the growth rate is real at the neutral point – the right hand side of (55) is a real valued function for k real. The problem, then, is to find the real roots (without loss of generality it is enough to look

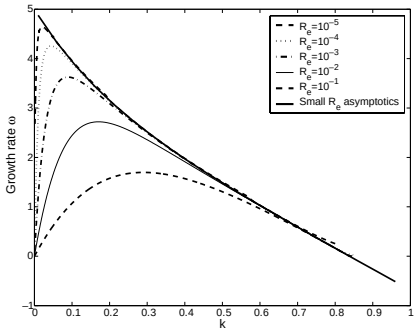

Figure 8. Stability characteristics as the Reynolds number tends to zero. Other parameters are fixed at $E_b = 10$, $\varepsilon_p = 4$ and $\sigma_R = 0{\cdot}5$. The asymptotic result (55) is shown by a bold solid curve.

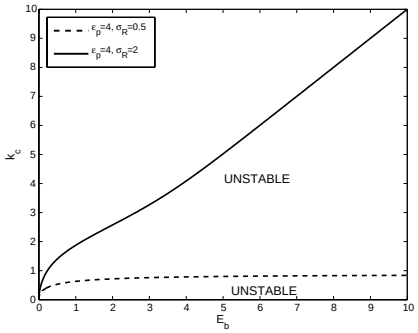

Figure 9. Neutral stability curves of critical wavenumber k_c vs. E_b for cases having $(\varepsilon_p\sigma_R - 1) > 0$ and (i) $(\sigma_R - 1)(1 - \varepsilon_p) > 0$ – dashed curve, and, (ii) $(\sigma_R - 1)(1 - \varepsilon_p) < 0$ – solid curve. The regions to the right of the curves are unstable and those above stable.

for $k > 0$) of the transcendental equation

$$E_b(\varepsilon_p\sigma_R - 1)ke^k = \sinh^2 k \cosh k \left[k(\tanh\sigma_R) + E_b(\sigma_R - 1)(1 - \varepsilon_p)\right]. \tag{58}$$

The asymptotic results (56) and (57) suggest that the cases $(\varepsilon_p\sigma_R - 1) > 0$ and $(\varepsilon_p\sigma_R - 1) < 0$ are different. In the former case, we expect a real positive root of (58) which measures the size of the instability band, and in the latter we will either have no roots (in which case the flow is stable for all k), or two distinct roots giving a band of unstable waves with a long wavenumber cut-off – as a physical parameter reaches a critical value, these two roots merge to give a monochromatic neutral wave. In what follows we quantify these observations and in particular we concentrate on varying E_b while keeping ε_p and σ_R fixed.

4.1.1. *The case* $(\varepsilon_p\sigma_R - 1) > 0$

The left-hand side (LHS) of (58) is positive and the right-hand side (RHS) is either positive or negative (for small k at least) depending on whether $(\sigma_R - 1)(1 - \varepsilon_p)$ is positive or negative, respectively. The former case is straight forward since the RHS is positive for all k, is much smaller than the LHS at small k, but much larger at large k, hence a root is guaranteed. If $(\sigma_R - 1)(1 - \varepsilon_p) < 0$, the RHS is negative for small k but again grows much faster than the LHS at large k, and again a positive root is obtained. The roots were found using Mathematica for two representative cases, (i) $\varepsilon_p = 4$, $\sigma_R = 0{\cdot}5$, and, (ii) $\varepsilon_p = 4$, $\sigma_R = 2$, and the neutral wavenumbers are plotted as a function of E_b in Figure 9. In both cases, we observe the $\sqrt{E_b}$ dependence near the origin that was shown earlier for order one R_e – see (53). The large E_b-dependence follows from (58) by noting that for case (i) the balance is between the LHS and the first term on the RHS, yielding $k_c \sim 1/2\log(E_b)$, while for case (ii) the balance is between the two terms on the RHS giving $k_c \sim E_b(\sigma_R - 1)(\varepsilon_p - 1)/(1 + \sigma_R)$. For the parameter values of Figure 9, the large E_b behavior is predicted to be $k_c \sim E_b$ and is in excellent agreement with the results.

4.1.2. *The case* $(\varepsilon_p\sigma_R - 1) < 0$

In this case, the criterion (48) is violated and as a consequence there are no unstable long waves; instability can only occur at finite k. If in addition we have $(\sigma_R - 1)(1 - \varepsilon_p) > 0$, then inspection of (58) shows that no real roots are possible for any E_b since the LHS is negative and the RHS is positive. A necessary condition for instability is therefore $(\sigma_R - 1)(1 - \varepsilon_p) < 0$,

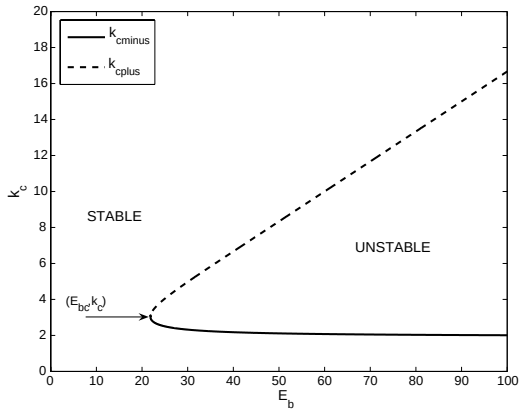

Figure 10. Neutral stability curves of critical wavenumber k_c *vs.* E_b for cases having $(\varepsilon_p\sigma_R - 1) < 0$ and $(\sigma_R - 1)(1-\varepsilon_p) < 0$. Solid curve is the lower neutral stability branch and the dashed curve is the upper neutral stability boundary. Parameter values are $\varepsilon = 0{\cdot}5$, $\sigma_R = 0{\cdot}5$. The region within the curve is unstable. The point $((E_{bc}, k_c) \approx (21{\cdot}81, 3{\cdot}035)$ denotes the nose where the neutral curves merge.

and the details depend on the values of the parameters. In particular, fixing ε_p and σ_R, we consider the effect of E_b. As mentioned above, we expect two neutral stability branches which will merge at a critical value of E_b. Such a situation has been calculated in Figure 10 for the values $\varepsilon_p = 0{\cdot}5$, $\sigma_R = 0{\cdot}5$. The solid curve represents the lower branch denoted by k_{cminus} and the dashed curve the upper branch denoted by k_{cplus}. We can see that the two branches merge at the point (E_{bc}, k_c) indicated on the figure. The particular values in this example are approximately equal to $(21{\cdot}81, 3{\cdot}035)$. We note that in the vicinity of the nose, a classical weakly nonlinear stability analysis is possible centered around the monochromatic neutral mode k_c.

5. Conclusions

We have formulated the nonlinear interfacial electrohydrodynamic problem of a viscous conducting liquid film of constant permittivity and conductivity, when a constant electric field is acting parallel to the film. The linear stability is studied and a dispersion relation is derived when the surrounding medium is hydrodynamically passive but conducting. The dispersion relation is valid in the limit when the charge relaxation time-scale is much smaller than the hydrodynamic time-scale, something that is usually found in practice and which has motivated several related studies (see [25,26,31]). We have studied the stability characteristics as each of the controling parameters is varied. The case of zero-Reynolds-number is considered in detail since it is more relevant in experiments (see [25] and the examples given in Section 2). In addition, asymptotic limits of long and short waves have been analyzed and used to confirm the calculations.

With inertia present, it is found that a general criterion for instability is the inequality $\varepsilon_p\sigma_R - 1 > 0$, and this becomes a necessary condition for instability to long waves. The effect of the electric field is felt through the electric Weber number E_b, and the maximum growth rate $\omega_{\max}$ along with the critical wavenumber k_c, decrease as E_b decreases to zero. We find that $\omega_{\max} \sim E_b$ and $k_c \sim \sqrt{E_b}$ as $E_b \to 0$ (Equation (53)) and these establish the scales to be used in studying the nonlinear response of the system near the bifurcation point $E_b = 0$. It is also established that when the conductivity of the surrounding medium increases relative to that of the fluid region, both $\omega_{\max}$ and k_c increase proportionally to σ_R (see Figure 4). A

decrease of σ_R causes $\omega_{\max}$ and k_c to decrease to zero at the rates $(\sigma_R - \sigma_{Rc})^{3/2}$ and $(\sigma_R - \sigma_{Rc})$, respectively, in the neighborhood of $\sigma_{Rc} = 1/\varepsilon_p$. As noted above for the variations in E_b, these rates in turn provide the appropriate asymptotic scalings that can be utilized in a study of the dynamics in the neighborhood of the bifurcation point $\sigma_R = \sigma_{Rc}$ – see Equation (54). The effect of the ratio of permittivities ε_p on the instability is similar to that for σ_R; that is, both $\omega_{\max}$ and k_c shrink to zero as $\varepsilon_p \to \varepsilon_{pc} = 1/\sigma_R$, while there is a proportional increase of both as ε_p increases (see Figure 5). This implies that the electric field enhances the instability of fluids which have higher permittivities, all other physical parameters held fixed. Variations in Reynolds number have also been calculated and as shown in Figure 6 the growth rate decreases with increasing R_e but the band of unstable waves remains finite.

The case $R_e = 0$ has been considered in detail. As indicated in the physical examples given in Section 2, typical values of R_e in related liquid bridge experiments are small with values of $0{\cdot}1$ at most (see [25]). This limit yields an explicit expression for the growth rate (see (55)), and consequently an expression for neutral wavenumbers (see (58)). The limiting form (55) is compared with the calculations (see Figure 8) and agreement is excellent; in fact the asymptotic result is valid as long as $k \gg R_e^{1/2}$ and a long wavenumber cut-off is achieved in a region $k \sim R_e^{1/2}$ as $R_e \to 0$, as indicated by the finite R_e numerical results (see also [33] for the related capillary thread problem). Neutral stability curves of k_c *vs.* E_b have been calculated and typical results are presented in Figures 9 and 10. The basic stability criteria can be summarized very simply as follows:

- $\varepsilon_p \sigma_R - 1 > 0$ is a *sufficient* but not necessary condition for instability. If this holds, the flow is unstable for all non-zero values of E_b. In addition, if the quantity $(\sigma_R - 1)(1 - \varepsilon_p)$ is positive/negative the band of unstable waves is smaller/larger respectively, for a given value of E_b (see Figure 9).
- $\varepsilon_p \sigma_R - 1 < 0$ can give instability only if in addition we have the criterion $(\sigma_R - 1)(1 - \varepsilon_p) < 0$. In such cases the flow is stable to all wavenumbers below a critical value E_{bc} and becomes unstable to a finite but growing band of wavenumbers as E_b increases above E_{bc} (see Figure 10).

These conclusions based on the results for Stokes flow broadly hold for non-zero R_e also. The main difference is that when $\varepsilon_p \sigma_R - 1 < 0$ and $(\sigma_R - 1)(1 - \varepsilon_p) < 0$, neutral stability is obtained at values of $E_b < E_{bc}$ where E_{bc} is analogous to that in Figure 10 – it can be seen from Figure 7 that the two corresponding neutral points when $R_e \neq 0$ vary in a similar way to the Stokes case, and as E_b is decreased a critical value E_{bc} is reached below which the instability disappears. Our numerical evidence suggests that for non-zero R_e the imaginary part of ω is also zero at this point and hence the principle of exchange of stabilities holds (we do not have a proof of this). Away from this point, ω is purely imaginary and asymptotes to the small k result (47) as k is reduced to zero.

In terms of dimensional quantities, the results above show that instability will be present at any electric field strength as long as $\varepsilon_{\text{in}}/\varepsilon_{\text{out}} > \sigma_{\text{in}}/\sigma_{\text{out}}$. If however $\varepsilon_{\text{in}}/\varepsilon_{\text{out}} < \sigma_{\text{in}}/\sigma_{\text{out}}$, then instability is possible only if $(\sigma_{\text{out}} - \sigma_{\text{in}})(\varepsilon_{\text{out}} - \varepsilon_{\text{in}}) < 0$. As mentioned earlier, this condition has been pointed out in [20] and has its origin in the polarization forces at the interface due to the permittivity contrast. We also note that this condition requires the more conducting fluid to have the lower permittivity, or the less conducting fluid to have the higher permittivity. This is usually difficult to achieve in practice – for example in the experiments of [25] the conductivities and permittivities of the pair of fluids of castor oil/eugenol and silicone oil 12 M are $2{\cdot}42 \times 10^{-9}$ Sm^{-1}, $5{\cdot}24\epsilon_{fs}$ and $1{\cdot}98 \times 10^{-12}$ Sm^{-1} and $2{\cdot}74\epsilon_{\text{fs}}$, where ϵ_{fs} is the permittivity of free space.

The detailed linear stability results presented here can be used to guide nonlinear studies in three directions. First, the weakly nonlinear stability analysis in the vicinity of the bifurcation points $E_b = 0$, $\sigma_R = \sigma_{Rc}$ and $\varepsilon_p = \varepsilon_{pc}$, as well as the corresponding analysis near the nose $E_b = E_{bc}$ when criterion (48) is violated. Second, a strongly nonlinear long wave theory as was successfully implemented in [9,11,18], and, third a full computational study to construct nonlinear traveling waves, for example, as well as the time evolution and possible rupture of the layer in the zero R_e limit where accurate boundary-integral methods can be used (see the analogous inviscid studies of [9,10]).These studies are the subject of current and future research.

Acknowledgements

DTP was supported by the National Science Foundation Grant DMS-0072228. PGP was supported by a Grant from the Air Force Office of Scientific Research, AFOSR Grant no. F49620-02-1-0031.

References

1. D. Gallez and M. Prevost, Linear and nonlinear dynamics of free-liquid films. *Physicochem. Hydrodyn.* 6 (1985) 731–745.
2. M. Prevost and D. Gallez, Nonlinear rupture of thin free liquid films. *J. Chem. Phys.* 84 (1986) 4043–4048.
3. C. Maldarelli, R.K. Jain, I.B. Ivanov and E. Ruckenstein, Stability of symmetric and unsymmetric thin liquid films to short and long wavelength perturbations. *J. Colloid Interface Sci.* 78 (1980) 118–143.
4. E. Ruckenstein and R.K. Jain, Spontaneous rupture of thin liquid films. *J. Chem. Soc. Faraday Trans. II* 70 (1974) 132–147.
5. R.K. Jain and E. Ruckenstein, Stability of stagnant viscous films on a solid surface. *J. Colloid Interface Sci.* 54 (1976) 108–116.
6. G.I. Taylor, The dynamics of thin sheets of fluid. II. Waves on fluid sheets. *Proc. R. Soc. London A* 253 (1959) 296–312.
7. W. Kinnersley, Exact large amplitude capillary waves on sheets of fluid. *J. Fluid Mech.* 77 (1976) 229–241.
8. D.G. Crowdy, Exact solutions for steady capillary waves on a fluid annulus. *J. Nonlinear Sci.* 9 (1999) 615–640.
9. D.T. Papageorgiou and J.-M. Vanden-Broeck, Large amplitude capillary waves in electrified fluid sheets. *J. Fluid Mech.* 508 (2004) 71–88.
10. D.T. Papageorgiou and J.-M. Vanden-Broeck, Antisymmetric capillary waves in electrified fluid sheets. To appear in *Eur. J. Appl. Math.* (2004).
11. B.S. Tilley, P.G. Petropoulos and D.T. Papageorgiou, Dynamics and rupture of planar electrified liquid sheets. *Phys. Fluids* 13 (2001) 3547–3563.
12. T. Erneux and S.H. Davis, Nonlinear rupture of free films. *Phys. Fluids A* 5 (1993) 1117–1122.
13. A. Sharma and E. Ruckenstein, Finite-amplitude instability of thin free and wetting films – prediction of lifetimes. *Langmuir* 2 (1986) 480–494.
14. M.P. Ida and M.J. Miksis, The dynamics of thin films I: General theory. *SIAM J. Appl. Math.* 58 (1998) 456–473.
15. M.P. Ida and M.J. Miksis, The dynamics of thin films II: Applications. *SIAM J. Appl. Math.* 58 (1998) 474–500.
16. M.P. Ida and M.J. Miksis, Thin film rupture. *Applied Math Letters* 9 (1996) 35–40.
17. D. Vaynblat, J.R. Lister and T.P. Witelski, Rupture of thin films by van der Waals forces: Evolution and self-similarity. *Phys. Fluids* 13 (2001) 1130–1140.
18. K. Savettaseranee, D.T. Papageorgiou, P.G. Petropoulos and B.S. Tilley, The effect of electric fields on the rupture of thin viscous films by van der Waals forces. *Phys. Fluids* 15 (2003) 641–652.
19. J.R. Melcher, *Field-coupled Surface Waves: A Comparative Study of Surface-coupled Electrohydrodynamic and Magnetohydrodynamic Systems*. Cambridge, MA: MIT Press (1963) 190 pp.

20. J.R. Melcher and W.J. Schwarz, Jr., Interfacial relaxation overstability in a tangential electric field. *Phys. Fluids* 11 (1968) 2604–2616.
21. J.R. Melcher and G.I. Taylor, Electrohydrodynamics: a review of the role of interfacial shear stresses. *Annu. Rev. Fluid Mech.* 1 (1969) 111–146.
22. D.A. Saville, Electrohydrodynamics: The Taylor–Melcher leaky dielectric model. *Annu. Rev. Fluid Mech.* 29 (1997) 27–64.
23. A.J. Mestel, Electrohydrodynamic stability of a slightly viscous jet. *J. Fluid Mech.* 274 (1994) 93–113.
24. A.J. Mestel, Electrohydrodynamic stability of a highly viscous jet. *J. Fluid Mech.* 312 (1996) 311–326.
25. C.L. Burcham and D.A. Saville, The electrohydrodynamic stability of a liquid bridge: Microgravity experiments on a bridge suspended in a dielectric gas. *J. Fluid Mech.* 405 (2000) 37–56.
26. C.L. Burcham and D.A. Saville, Electrohydrodynamic stability: Taylor–Melcher theory for a liquid bridge suspended in a dielectric gas. *J. Fluid Mech.* 452 (2002) 163–187.
27. A. Castellanos and A. Gonzalez, Nonlinear electrohydrodynamics of free surfaces. *IEEE Trans. Dielectr. Electr. Insul.* 5 (1998) 334–343.
28. J.D. Jackson, *Classical Electrodynamics*. New York: John Wiley and Sons (1963) 641 pp.
29. D.T. Papageorgiou, Hydrodynamics of surface tension dominated flows. In: M.G. Velarde and R.K. Zeytounian (eds), *Interfacial Phenomena and the Marangoni Effect*. CISM Courses and Lectures 428. Wien, NY: Springer (2002) pp. 41–88.
30. C. Pozrikidis, Interfacial dynamics for Stokes flow. *J. Comp. Phys.* 169 (2001) 250–301.
31. N.A. Pelekasis, K. Economou and J.A. Tsamopoulos, Linear oscillations and stability of a liquid bridge in an axial electric field. *Phys. Fluids* 13 (2001) 3564–3581.
32. S. Tomotika, On the stability of a cylindrical thread of a viscous liquid surrounded by another viscous fluid. *Proc. R. Soc. London A* 150 (1935) 322–337.
33. M.-L.E. Timmermanns and J.R. Lister, The effect of surfactant on the stability of a liquid thread. *J. Fluid Mech.* 459 (2002) 289–306.